Journal of
Materials Chemistry C

Accepted Manuscript

This is an *Accepted Manuscript*, which has been through the RSC Publishing peer review process and has been accepted for publication.

Accepted Manuscripts are published online shortly after acceptance, which is prior to technical editing, formatting and proof reading. This free service from RSC Publishing allows authors to make their results available to the community, in citable form, before publication of the edited article. This *Accepted Manuscript* will be replaced by the edited and formatted *Advance Article* as soon as this is available.

To cite this manuscript please use its permanent Digital Object Identifier (DOI®), which is identical for all formats of publication.

More information about *Accepted Manuscripts* can be found in the **Information for Authors**.

Please note that technical editing may introduce minor changes to the text and/or graphics contained in the manuscript submitted by the author(s) which may alter content, and that the standard **Terms & Conditions** and the **ethical guidelines** that apply to the journal are still applicable. In no event shall the RSC be held responsible for any errors or omissions in these *Accepted Manuscript* manuscripts or any consequences arising from the use of any information contained in them.

RSC Publishing

www.rsc.org/materialsC

Registered Charity Number 207890

Journal of Materials Chemistry C

Dynamic Article Links ►

Cite this: DOI: 10.1039/c0xx00000x

www.rsc.org/xxxxxx

communication

Highly stable solution-processed ZnO thin film transistors via simple Al evaporation process

Tae Sung Kang[a], Tae Yoon Kim[a], Gyu Min Lee[b], Hyun Chul Sohn[b], and Jin Pyo Hong*[a]

Received (in XXX, XXX) Xth XXXXXXXXX 20XX, Accepted Xth XXXXXXXXX 20XX
DOI: 10.1039/b000000x

Amorphous metal oxide thin film transistors (TFTs) are expected to serve as building blocks in a variety of devices, such as bendable displays, transparent mobile phones, and plastic newspapers. Here, we report a simple approach for highly stable solution-based zinc oxide (ZnO) TFTs by simply evaporating Al on the back channel layer without any additional chemical or plasma processes for passivation. In particular, control and manipulation of Al nanoparticle (NP) formation represents one of the key approaches in this work. The possible sketch of the improved nature is proposed, along with various structural and electrical analyses.

Metal oxide semiconductor thin film transistors (TFTs) have garnered considerable interest as alternatives to conventional amorphous silicon-based TFTs due to their high electrical mobility, transparency in visible light, and high on/off ratio.[1,2] Therefore, a variety of vacuum deposition methods ensuring outstanding electrical features, such as radio frequency (RF) sputtering, pulsed laser deposition, and atomic layer deposition, have been extensively employed.[3-5] In recent years, solution-processed TFTs have also become highly promising options for use in simple processes, thus enabling the fabrication of low cost electronics.[6,7] Suitable materials tested included various solution-processed metal alloys such as ZnO, InZnO, ZnSnO, and InGaZnO.[8-10] Kim *et al.* demonstrated that the deep-ultraviolet irradiation method induced efficient condensation and densification of solution-based channel layers with photochemical activation, resulting in improved electrical behavior.[11] Park's work reported that a carbon-free zinc ammonia complex solution with alkali metal dopants exhibited a drastic reduction of residual carbon impurities and improved electrical performance.[12] Much effort, including various dopant techniques and fabrication methods, has been dedicated towards the electrical improvement of metal oxide TFT devices; however, TFTs have been inherently hindered by the environmental atmosphere, which affects device stability. Particularly, the solution-based TFTs surrounding the atmosphere are highly susceptible to unintended device instability due to the spatial trap states induced by inherently vulnerable metal-oxygen bonding structures.[13,14] In addition, it is well known that nano-size pores build up on the metal oxide channel layer from metallic precursors during annealing, leading to device instability due to significantly increased charge-trapping sites acting as defect states.[15-18] Therefore, manipulation of device stability is one of the key challenges concerning the requirements of high-performance display applications. The passivation concept that addresses atmospheric problems was tested with HfO_2, SiO_2, SiN, and Al_2O_3 layers on the back channel surface.[19,20] However, these additional processes have always required the use of chemicals or plasma along with highly sophisticated processing conditions (e.g., temperature, pressure, and gas atmosphere). Thus, practical questions still remain regarding unintended chemical reaction at the interface between the passivation layer and active layer during the passivation process, which results in degradation of electrical performance.

In this letter, we report an effective Al evaporation approach for highly stable solution-based ZnO TFTs, where our device process does not require any additional chemical or plasma processes for passivation. We describe the electrical and structural features of various solution-based ZnO TFTs extensively. The possible nature of the improved device stability is proposed by employing the formation of Al nanoparticles (NPs) on the back channel of a ZnO film and a partial Al atom (ion) impregnation process.

The precursor solution was prepared by dissolving 0.01 M zinc oxide (Aldrich 99.99%) in 10 mL ammonium hydroxide (Aldrich 99.99%). To increase the solubility of ZnO powder, the precursor was stored in a refrigerator for one day because the ZnO particles easily precipitate in the precursor solution at room temperature. Before the deposition process, thermally-grown 200-nm SiO_2 on the heavily B-doped, n-type Si (resistivity below 0.005 Ωcm) substrate was cleaned with a piranha solution (H_2O_2 : H_2SO_4 = 1 : 1) and was dipped into diluted HF for 1 min to remove the residual sulfur. As-prepared SiO_2/Si substrate was treated with ultraviolet ozone for 30 s to make the surface hydrophilic so that the precursor could be deposited more effectively. The prepared ZnO solution was deposited by a spin coating process for 60 s at 3000 rpm with a thickness of 8–10 nm. As soon as the film was spin-coated, it was annealed on a hotplate for 1 h at 300 °C to remove the solvents. After deposition of the ZnO layer, Al nanoparticles with sizes of approximately 7-11 nm were subsequently deposited on ZnO films under 10^{-7} Torr by thermal evaporation at room temperature. The deposition rate of Al was

Journal of Materials Chemistry C Accepted Manuscript

0.3 Å/sec. Finally, the Al source/drain (S/D) region was thermally deposited on the active layer via a shadow mask. The channel width (W) and length (L) were 500 and 50 μm, respectively. Current-voltage (I-V) characteristics were determined using a Keithley 4200-Semiconductor Characterization System (4200-scs) with a probe station.

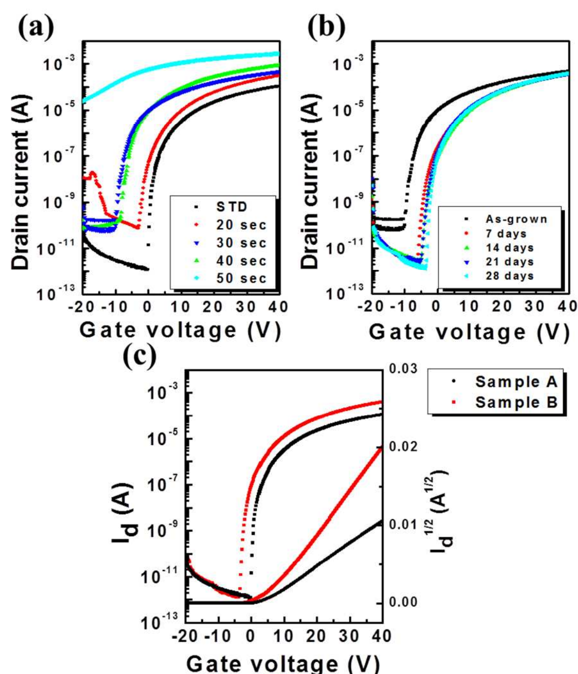

Fig. 1 Current-voltage features of pure ZnO(STD) and Al-evaporated ZnO TFTs. (a) Transfer characteristic curves of pure ZnO and Al-evaporated ZnO TFTs as a function of Al deposition time ranging from 0 to 50 sec at a fixed drain voltage of 10 V. All the Al-evaporated ZnO TFTs demonstrated negative shifts in the V_{th} compared to pure ZnO TFTs; these shift may come from the increase in carrier concentration under Al evaporation. (b) Electrical responses of the Al-evaporated ZnO TFT optimized at 40 sec. The sample was exposed to air for approximately one month. At first, relatively large positive V_{th} shifts were provided in a short exposure time and were then followed by a slight shift of V_{th} after a certain exposure time. (c) Compared transfer characteristic representation of pure ZnO (Sample A) and Al-evaporated ZnO TFT (Sample B) optimized at 40 sec.

Fig. 1a plots the representative drain-gate I-V curves of ZnO TFTs with Al evaporated at different deposition times ranging from 0 to 50 sec, where the deposition rate is fixed at 0.3Å/sec. All of the samples exhibited typical n-channel behavior. More detailed geometric layouts of Al-evaporated ZnO TFTs grown on SiO_2/Si substrates are given in Supporting Information Fig. S1†. As shown in Fig. 1a, the drain current (I_d) at a fixed gate voltage (V_g) was gradually increased up to a 40 sec deposition time, providing improved electron transport with a negative shift (ΔV_{th}) in the threshold voltage (V_{th}). The negative ΔV_{th} under deposition of Al on ZnO may occur due to an increase in carrier concentration since the charge density in the channel layer is directly related to V_{th}.[21] This can be explained by the electron injection from Al into ZnO due to the work function difference.[22] This increased carrier concentration reduces potential barriers above the conduction band minimum, thus enhancing electron mobility.[23] However, the Al-evaporated ZnO TFT prepared at 50 sec allowed for an abrupt increase in I_d with a decreased on/off ratio, as shown in Fig. 1a. Therefore, we expect that a short Al deposition time up to 40 sec might drive the formation of Al NPs on the back channel surface of the ZnO film due to a different surface energy at the Al/ZnO interface. Al has a relatively high surface energy per unit area compared to that of the ZnO layer.[24,25] On the other hand, a relatively long Al deposition time (50 sec) could correspond to the presence of an Al metal thin film, not the appearance of Al NPs created by a short Al deposition time. Thus, current flows through an Al metal film on the back channel of the ZnO layer, providing large leakage current paths between the source and drain. More detailed transfer curves of ZnO TFTs provided by different Al deposition times are shown in Supporting Information Fig. S2†. After several samples were systematically examined, a relatively optimized Al-evaporated ZnO TFT prepared at 40 sec was selected for a reliability test. As plotted in Fig. 1b, the initial electron mobility of the as-grown sample just after fabrication was about 7.82 cm^2/V s. When the sample was exposed to air for about one month, the V_{th} was shifted positively from -6.61 V to +3.14 V, and the mobility was decreased from 7.82 cm^2/V s to 5.79 cm^2/V s with decreased subthreshold swing (S.S) values. This positive ΔV_{th} under air exposure might be the consequence of the reduction of excess carrier concentrations.[26] The nature of reduced carrier concentrations under exposure to air will be explained later. Fig. 1c displays the transfer characteristics of pure ZnO TFTs without Al (Sample A) and with Al evaporated for 40 sec (Sample B). Sample B provided a field effect mobility (5.79 cm^2/V s) greater than that of Sample A (1.603 cm^2/V s).

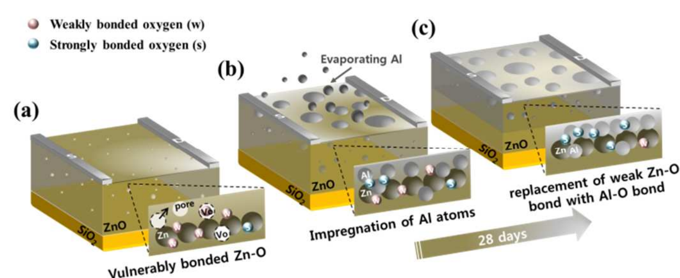

Fig.2 Schematic device architectures of pure ZnO and Al-evaporated ZnO TFTs. (a) Typical schematic of pure ZnO TFTs without Al evaporation on the back channel surface of the ZnO layer, where natural pore structures are possibly formed during solution processing. (b) Schematic illustration of Al-evaporated ZnO TFTs, suggesting the impregnation of thermally activated Al atoms or ions into the ZnO layer providing electron injection, resulting in a positively shifted V_{th} compared that of pure ZnO TFTs. (c) Schematic of time-dependent Al-evaporated ZnO TFTs under air exposure for one month, where the replacement of weak Zn-O bonds with Al-O bonds takes place.

In order to predict the role of Al evaporation on the back channel surface of the ZnO layer, we used Al atom or ion impregnation during evaporation and the roles of Al NPs remaining on the back channel surface of the ZnO layer are described as above. Fig. 2 illustrates how Al evaporation possibly influences electrical performance using three samples: Sample A without Al evaporation (pure sample), Sample B prepared at 40 sec, and Sample C prepared as Sample B but exposed to air for one month. Shown in Fig. 2a, Sample A consists of weak Zn-O bonds that are associated with the oxygen defects created by

Journal of Materials Chemistry C Accepted Manuscript

 This journal is © The Royal Society of Chemistry [year]

naturally formed pore structures during ZnO fabrication. However, when Al is evaporated on Sample A at a proper deposition time (40 sec), thermally-activated Al atoms or ions from the back channel surface partially penetrate or impregnate the ZnO layer during evaporation and partially remain on the back channel surface of ZnO as Al NPs (Fig. 2b).[27,28] Thus, at first, electron injection from impregnated Al atoms inside the ZnO channel layer occurs, corresponding to increased charge density. This electron injection may be described by the difference in the work functions between the Al and ZnO layers, where the work function of Al is less than the conduction band of ZnO.[22] Theoretical calculations predict Al atomic diffusion towards crystalline solids via a vacancy mechanism because the formation energy of a vacancy in n-type ZnO is relatively small.[29] As described above, impregnated Al atoms or ions inside the ZnO layer generate Al-O bonds with oxygen ions since the Al atoms have a greater reduction potential than Zn atoms (Fig. 2c).[30] In addition, the generated Al-O bonding may also produce the possible formation of AlZnO film, which permits the band gap to increase since it is well-known that the optical band gap of AlZnO film is larger than that of ZnO.[31] Therefore, a AlZnO/ZnO hetero-junction system takes place, allowing a potential well to accumulate electrons and to cause a high electron mobility.[32,33] However, after reaching the thermal equilibrium state between Al and AlZnO, it should be noted that the Al-O bonding can cause the occurrence of an energy band bending in the AlZnO film to move upward. Therefore, the accumulated electron density in energy well would decrease, inducing a positive V_{th} shift due to a reduction of total charge concentration. (see Fig S4 in the ESI†)

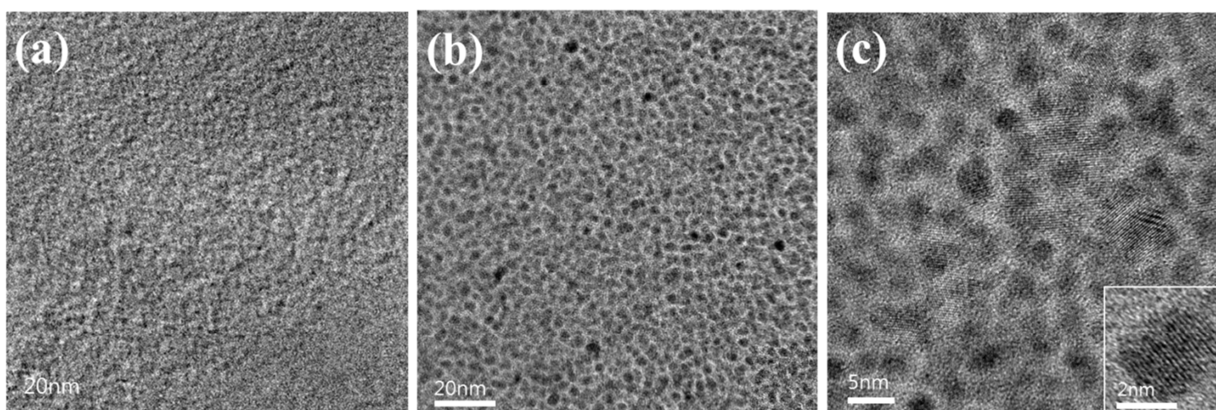

Fig. 3 Structural TEM images of Sample A and B. Top plane views of (a) a pure (Sample A) and (b) Al-evaporated for 40sec on ZnO (Sample B) showing distributed Al NPs.(c) The size of the Al particle was approximately 4–6 nm as shown the inset of fig. 3c.

A closer microstructural investigation of Sample A and B was performed using a transmission electron microscope (TEM) for comparison. Fig. 3a presents a typical surface image of Sample A, indicating the presence of rough morphologies on the solution-processed metal oxide channel surface. Fig. 3b illustrates the appearance of distributed Al NPs on the back channel surface of ZnO (Sample B). The inset of Fig. 3c displays an Al NP image with a size of approximately 5 nm.

To further study the element distribution inside Sample A and B, the cross-sectional energy dispersion X-ray spectroscopy (EDS) mappings were taken. Fig. 4a reveals a high-angle annular dark-field (HAADF) scanning TEM (STEM) image of Sample A. Fig. 4b and 4c indicate the EDS elemental mappings of Zn and Al, respectively. As shown in this figure, the Al atoms were not detected for Sample A. Similarly, the HAADF-STEM image for Sample B is shown in Fig. 4d and the EDS elemental mappings of Zn and Al are displayed in Fig. 4e and 4f, respectively. As expected, the Al atoms were clearly detected inside the ZnO layer. An atomic depth-profile was also observed, as shown in Supporting Information Fig. S3†.

In order to further predict the metal-oxygen bonding of Sample B, the defects associated with oxygen deficiencies were examined using an X-ray photoelectron spectroscopy (XPS) depth profile analysis. The XPS spectrum was calibrated by using the binding energy of the C 1s peak (285.0 eV) as a reference, and the Ar sputtering etching rate was approximately 3 nm/min at 2×10^{-8} Torr. In addition, in order to estimate the atomic concentration, the depths induced by various Al deposition times were also determined by secondary ion mass spectroscopy (SIMS) (see Fig. S5 in the ESI†).

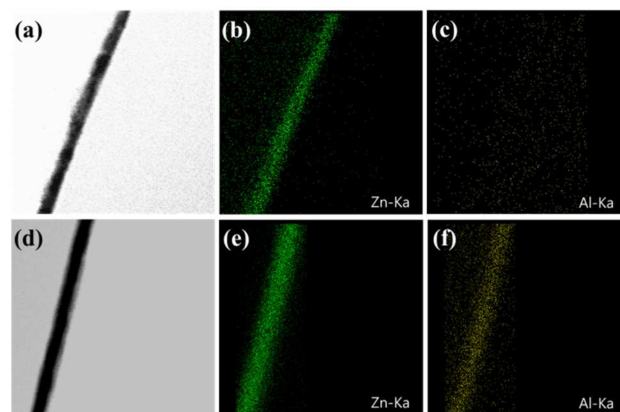

Fig. 4 Cross-sectional STEM-HAADF image of (a) Sample A and EDS elemental mapping data of (b) Zn and (c) Al. In the same manner, (d) Cross-sectional image of Sample B and EDS element mapping data of (e) Zn and (f) Al indicating that Al atoms were impregnated into the ZnO channel layer.

Journal of Materials Chemistry C Accepted Manuscript

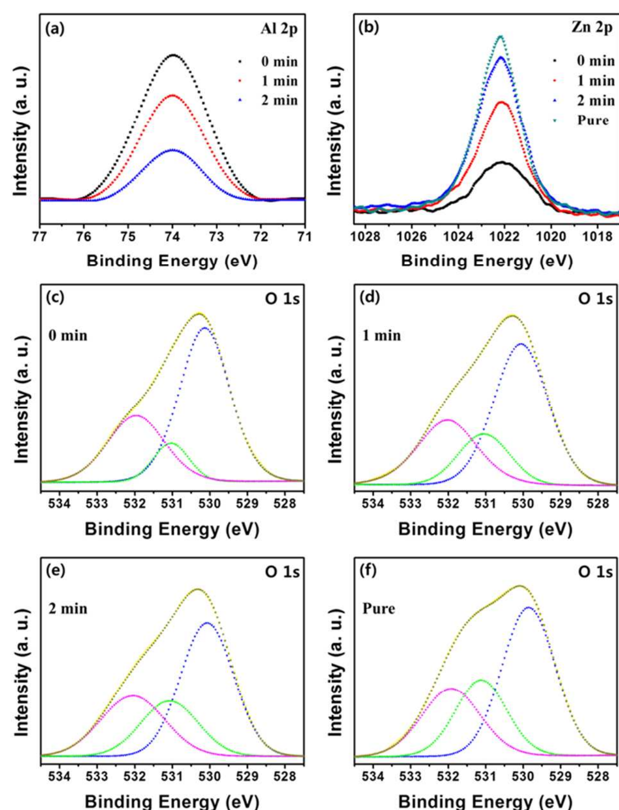

Fig. 5 XPS depth profiles of Sample B. The various intensities of (a) Al and (b) Zn binding energies were presented with Ar sputtering (3nm/min). The O1s XPS spectra were subsequently analyzed depending on etching time: (c) 0, d) 1, and (e) 2 min, followed by (f) the oxygen peak of fairly pure ZnO as the etching time increased beyond 2 min.

Figs. 5a and 5b show the XPS spectra of Al 2p3/2 and Zn 2p3/2 at various depths for Sample B, respectively. The Al peak was clearly verified at up to 2 minutes of etching, which was approximately 6 nm, after which the Al component was not detected. For Al, a binding energy of 73.98 eV was observed for all depths by the Ar etching process, suggesting the presence of dominant Al oxidation states.[34] In contrast, the Zn 2p3/2 peak (1022.10 eV) gradually increased with etching time, and slightly shifted towards a higher binding energy from 1022.10 eV to 1022.30 eV in Sample B. This peak shift may represent the appearance of Al-O binding, rather than that of weakly bonded Zn-O near the surface.[35] The removal of weakly bonded oxygen from the Zn-O bond is shown in Figs. 5c, 5d, 5e, and 5f for the O 1s XPS spectra with various etching depths. In these figures, the O 1s binding energy of each figure was de-convoluted into three peaks, corresponding to the low binding peak (P_L), medium binding peak (P_M), and high binding peak (P_H) at ~530.2, ~531.2, and ~531.9 eV, respectively. The peaks centered at 530.2 ± 0.3 eV and 531.2 ± 0.3 eV were assigned to oxygen atoms in the oxide lattice without and with oxygen vacancies, respectively. The peak at 531.9 ± 0.3 eV could originate from surface oxygen such as hydroxyl groups.[36] The relative intensity ratio of the medium-binding energy component ($P_M/P_L+P_M+P_H$) increased from 10.41% to 28.78% as the etching time increased. For O 1s, the peak energy at 531.2 eV refers to oxygen bonds associated with defects such as oxygen vacancies. The reduction of defect-related vacancies may occur from the difference in standard electrode potentials (SEPs) between Al and Zn ions of -1.662 and -0.76 V, respectively.[30] The large SEP of Al ions means that they easily experience oxidation so that the Al^+ ion can provide stronger and more rigid bonding to oxygen ions than Zn-O bonds.

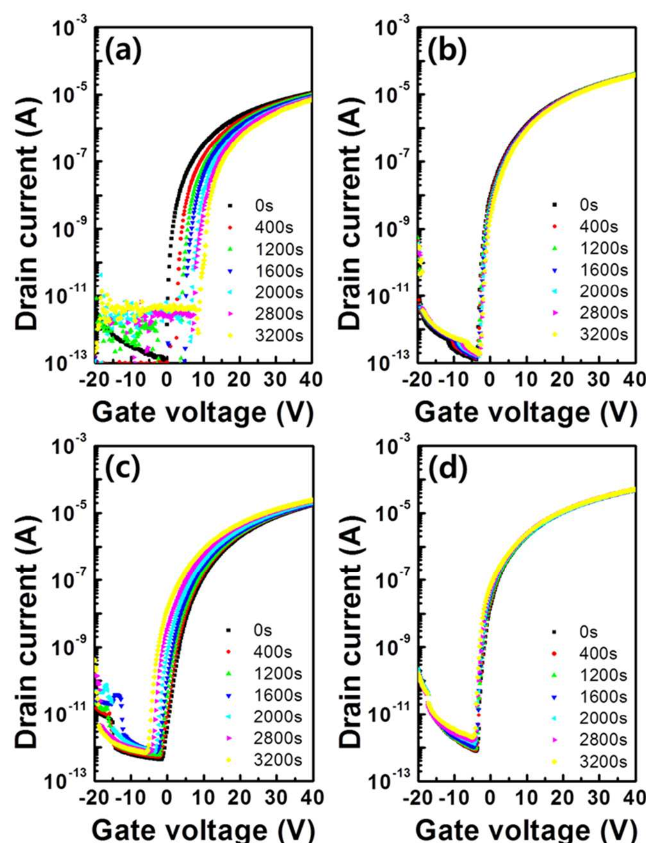

Fig. 6 Transfer characteristics for (a) Sample A and (b) Sample B versus PBS time, and transfer characteristics of (c) Sample A and (d) Sample B versus NBIS time, where the transfer curves during stress were taken at a fixed drain voltage of 10 V at room temperature.

Electrical responses under positive bias stress (PBS) and negative bias illumination stress (NBIS) for Samples A and B were also conducted, as represented in Fig. 6. Fig. S6† shows the summarized ΔV_{th} for both samples versus stress time. As a first step, a positive bias of +20 V was applied to the gate electrode and the maximum stress time was 3200 s for the PBS (Figs. 6a and 6b). Transfer curves of Sample A exhibited a large positive ΔV_{th} (~ +8.59 V) with increasing stress time. In contrast, Sample B displayed a much smaller positive change in ΔV_{th} (~ +0.86 V), which was a 90 % decrease in the $\Delta V_{th}/\Delta V_o$ compared to Sample A. Previous works reported that solution-based TFTs suffered from strong oxygen adsorption due to the presence of unintended porous structures.[15,16] This porous matrix could be easily generated by the escaped precursors during annealing, corresponding to the irreversible creation of pore-related oxygen vacancies.[17,18] Furthermore, the adsorption of oxygen molecules on the exposed back-channel surface can deplete the electron carriers of the ZnO channel layer due to the large electronegativity of the oxygen molecules, leading to a positive ΔV_{th}.[37] Therefore, we expect that the proper Al-evaporated ZnO layer allowed for the reduction of trap sites created by the

Journal of Materials Chemistry C Accepted Manuscript

This journal is © The Royal Society of Chemistry [year]

initially porous ZnO layer and also allowed for a decrease in the interaction between the back channel surface and oxygen under an ambient atmosphere. Figs. 6c and 6d show the stability test under NBIS. Similarly, a negative bias of -20 V was applied to the gate electrode with the same stress duration. The samples were illuminated with light (~2.0 mW/cm^2) at a wavelength of ~500 nm, which was filtered from a white-light halogen lamp. Sample A experienced a large negative ΔV_{th} (~ -5.92 V) after the NBIS, whereas Sample B stayed relatively stable (~ -0.91 V), experiencing an 84% decrease in $\Delta V_{th}/\Delta V_o$. In addition, as shown in this figure, the V_{th} shifted, but the field effect mobility and S.S variation remained stable. This behavior may be understood in terms of charge trapping rather than charge injection into the gate dielectric bulk region; this charge trapping is related to the photo-desorption of O_2 on the channel surface and the V_o concentration in the ZnO layer.[38] As a result, Al NP-passivated ZnO TFTs can reduce pre-existing vacancy-related defects, thus enabling improved stability.

In conclusion, we introduce a simple Al evaporation method as an alternative solution for highly stable, solution-processed ZnO TFTs. In particular, passivation was eliminated in our process. The structural and chemical compositions including defect-related oxygen vacancies were examined extensively. The origin of the highly stable electric characteristics seems to be attributable to the combined effect of Al atom or ion impregnation on the ZnO layer, which provide electron injection by different work functions, and the formation of Al NPs on the back channel of ZnO layer, which serve as a passivation layer. In addition, the positively shifted V_{th} with respect to air exposure time is associated with moving upward energy well at AlZnO/ZnO interface due to thermal equilibrium after oxidation of Al. In particular, reasonable stability of solution-processed ZnO TFTs under long-term bias stress is essential to this work, as is the improved field effect mobility of 5.79 cm^2/V s and the on/off current ratio of ~10^8. Our metal evaporation approach on the back channel surface of solution-based TFTs may establish a useful and simple route for highly stable TFTs.

Acknowledgements

This research was supported by the Converging Research Center Program funded by the Ministry of Education, Science and Technology (Project No. 2011K000877).

Notes and references

[a] *Department of Physics, Hanyang University, Seoul, 133-791, South Korea, Fax :+82-2-2295-6868; Tel : +82-2-2220-0911; E-mail : jphong@hanyang.ac.kr*
[b] *Department of Material Science and Engineering, Yonsei University, Seoul, 120-749, South Korea*

† Electronic supplementary information (ESI) available: The Schematic of solution-processed ZnO TFTs passivated by Al NPs, the electrical characteristics of Al evaporated ZnO-TFTs with various deposition time, EDS, SIMS, and V_{th} shift under stress time data for ZnO thin flms. See DOI: 10.1039/c000000x/

1 K. Nomura, H. Ohta, A. Takagi, T. Kamiya, M. Hirano, Hideo Hosono. *Nature* **2004**, *432*, 488.
2 H. Yabuta, M. Sano, K. Abe, T. Aiba, T. Den, H. Kumomi, K. Nomura, T. Kamiya, H. Hosono, *Appl. Phys. Lett*. **2006**, *89*, 112123.
3 P. F. Carcia, R. S. McLean, M. H. Reilly, G. Nunes, *Appl. Phys. Lett*. **2003**, *82*, 1117
4 S. Masuda, K. Kitamura, Y. Okumura, S. Miyatake, *J. Appl. Phys. 2003, 93,1624*
5 D. H. Levy, D. Freeman, S. F. Nelson, P. J. Cowdery-Corvan, L. M. Irving, *Appl. Phys. Lett*. **2008**, *92*, 192101
6 S. T. Meyers, J. T. Anderson, C. M. Hung, J. Thompson, J. F. Wager, D. A. Keszler, *J. Am. Chem. Soc.* **2008**, *130*, 17603.
7 B. S. Ong, C. Li, Y. Li, Y.Wu, R. Loutfy, *J. Am. Chem. Soc*. **2007**, *129*, 2750.
8 C. G. Choi, S.-J. Seo, B.-S. Bae, *Electrochem. Solid-State Lett*. **2008**, *11*, H7.
9 Y. H. Yang, S. Yang, K. S. Chou, *IEEE Electron Device Lett*. **2010** , *31* , 969.
10 C. Avis, J. Jang, *J. Mater. Chem*. **2011**, *21*, 10649.
11 Y. H. Kim, J. S. Heo, T. H. Kim, S. Park, M. H. Yoon, J. Kim, M. S. Oh, G. R. Yi, Y. Y. Noh, S. K. Park, *Nature* **2012**, *489*, 128.
12 S. Y. Park , B. J. Kim , K. Kim , M. S. Kang , K. H. Lim , T. Il Lee , J. M. Myoung , H. K. Baik , J. H. Cho , Y. S. Kim , *Adv. Mater.* **2012** , *24* , 834.
13 M. Ortel, S. Pittner, V. Wagner, *Appl. Phys. Lett*. **2013**, *113*, 154502.
14 D. Gupta, S. Yoo, C. Lee, Y. Hong, *IEEE Transactions on Electron Devices* **2011**, *58*, 1995.
15 Y. Jeong, K. Song, D. Kim, C. Y. Koo, J. Moon, *J. Electrochem. Soc*. **2009**, *156*, H808.
16 C. Bae, D. Kim, S. Moon, T. Choi, Y. Kim, B. S. Kim, J. S. Lee, H. Shin, J. Moon, *Acs Applied Materials &Interfaces* **2010**, *2*, 626.
17 D. H. Lee, Y. J. Chang, W. Stickle, C. H. Chang, *J. Electrochem. Soc.* **2007**, *10,* K51.
18 C. Li, Y. Li, Y. Wu, B. S. Ong, R. O. Loutfy, *J. Mater. Chem.,* **2009**, *19,* 1626
19 J. S. Park, T. S. Kim, K. S. Son, K. H. Lee, W. J. Maeng, *Appl. Phys. Lett*. **2010**, *96*, 262109.
20 K. Nomura, T. Kamiya, H. Hosono, *Thin Solid Films*. **2012**, *520*, 3778.
21 N. L. Dehuff, E. S. Kettenring, D. Hong, H. Q. Chiang, J. F. Wager, R. L. Hoffman, C. H. Park, D. A. Keszler, *J. Appl. Phys*. **2005**, *97*, 064505.
22 H. W. Zan, W. T. Chen, C. C. Yeh, H. W. Hsueh, C. C. Tsai, H. F. Meng, *Appl. Phys. Lett.* **2011**, *98*, 153506.
23 T. Kamiya , K. Nomura , H. Hosono , *J. Displays Technol.* **2009** , *5* , 462 .
24 Q. Zhang, T. Cagˇın, A. Duin, W. A. Goddard III, *Phys. Rev. B* **2004** , *69* , 045423.
25 N. L. Marana, V. M. Longo, E. Longo, J. B. L. Martins, J. R. Sambrano, *J. Phys. Chem. A* **2008,** *112,* 8958.
26 R. M. Pasquarelli, D. S. Ginley, R. O'Hayre*, Chem. Soc. Rev*. **2011**, *40*, 5406.
27 R. Freer, *J Mater Sci* **1980**, 15, 803
28 V. J. Norman, *Aust. J. Chem* **1969**, *22*, 325
29 G. Y. Huang, C. Y. Wang, J. T. Wang, *J. Appl. Phys*. **2009**, *105*, 073504.
30 P. Vanysek, 'Electrochemical Series' in *Handbook of Chemistry and Physics*, 87th Ed (Ed: D. R. Lide), CRC Press, Boca Raton, FL, USA **2006**.
31 B. E. Sernelius, *Phys. Rev. B* **1988,** *37*, 10244
32 S. Y. Cheng, *Semicond. Sci. Technol.* **2002**, *17*, 701
33 H. W. Zan, C. C. Yeh, H. F. Meng, C. C. Tsai, L. H. Chen, *Adv.Mater.* **2012**, *24*, 3509
34 M. Chen, Z. L. Pei, C. Sun, L.S. Wen, X. Wang, *J. Cryst. Growth* **2000** , *220* , 254.
35 M. N. Islam, T. B. Ghosh, K. L. Chopra, H. N. Acharya, *Thin Solid Films.* **1996**, *280*, 20.
36 M. G. Kim, H. S. Kim, Y. G. Ha, J. He, M. G. Kanatzidis, A. Facchetti, T. J. Marks, *J. Am. Chem. Soc.* **2010**, *132*, 10352.
37 J. K. Jeong, H. W. Yang, J. H. Jeong, Y. G. Mo, H. D. Kim, *Appl. Phys. Lett.* **2008**, *93*, 123508.
38 K. H. Ji, J. I. Kim, H.Y. Jung, S.Y. Park, R. Choi, U. K. Kim, C. S. Hwang, D. Lee, H. Hwang, J. K. Jeong, *Appl. Phys. Lett*. **2011**, *98*, 103509.

Journal of Materials Chemistry C Accepted Manuscript